Received August 7, 2021, accepted August 15, 2021, date of publication August 30, 2021, date of current version September 10, 2021.

Digital Object Identifier 10.1109/ACCESS.2021.3108808

A Time-Delay Overlapping Modulation-Based High Spectral Efficiency and Secure DCSK System

XINYU DOU[1], XIAOHUI CHEN[1], DEQUN LIANG[1], AND BIN LIN[1,2], (Senior Member, IEEE)
[1]College of Information Science and Technology, Dalian Maritime University, Dalian 116026, China
[2]Peng Cheng Laboratory, Network Communication Research Centre, Shenzhen 518052, China

Corresponding author: Bin Lin (binlin@dlmu.edu.cn)

This work was supported in part by the National Key Research and Development Program of China under Grant 2019YFE0111600; in part by the National Natural Science Foundation of China under Grant 62001077, Grant 61801074, Grant 61971083, and Grant 51939001; in part by China Postdoctoral Science Foundation funded project under Grant 2019M661075; and in part by Dalian Science and Technology Innovation Fund under Grant 2019J11CY015.

ABSTRACT In this paper, a new high spectral efficiency differential-chaos-shift-keying system based on the time-delay overlapping modulation technology (TDOP-DCSK) is proposed. In this system, the binary bits are conveyed by multiple chaotic carriers which are delayed in turn and overlapped directly in time domain, and demodulated via solving the equation system. Benefiting from the time-delay overlapping modulation, TDOP-DCSK can offer higher spectral efficiency, data transmission rate and energy efficiency. Meanwhile, as multiple information-bearing chaotic signals are delayed and overlapped, the correlation between the reference and information-bearing signal is weakened, which brings a higher security level. The spectral efficiency, energy efficiency and security are analyzed, and the analytical BER expressions are derived over both additive white Gaussian noise (AWGN) and multipath Rayleigh fading channels. In addition, effects of various system parameters on the system performance are discussed, and the BER comparison between TDOP-DCSK and the traditional DCSK system is implemented to discover the means of TDOP-DCSK symbol constitution. The simulation results verify superiorities and show broad prospects of TDOP-DCSK.

INDEX TERMS Chaotic communication, time-delay overlapping modulation (TDOP), ill-condition, high spectral efficiency, security.

I. INTRODUCTION

Due to numerous superior inherent characteristics of chaotic signals such as noise-like wavelet, sensitive dependence on initial conditions, low probability of intercept, and δ-like self-correlation functions, the chaos-based communication technology has been widely applied in many communication scenarios, for instance, multi-user spread-spectrum communications, ultra-wideband systems (UWB), power-line communications, cognitive radio systems and secure communication systems [1]–[5].

Among various chaos-based communication systems, the differential chaos-shift-keying (DCSK) system has drawn extensive attention due to its simple system structure and outstanding anti-multipath interference ability [1]. Owing to the transmitted-reference (T-R) scheme, DCSK has two drawbacks to be overcame. One is the low spectral efficiency and data rate, because half of the bit duration is used to transmit the reference chaotic signal. The other is the weakened information security. Though the T-R scheme can avoid the implementation of chaos synchronization and channel state estimation, the information-bearing signal is easy to be intercepted and decrypted based on the reference chaotic signal sent at the same time.

With more and more electronic devices are accessing the communication network, both the transmission rate and the security of information are two urgent problems for DCSK systems. Therefore, various high data rate, high spectral efficiency, and high security level DCSK systems have been demonstrated over the last decades. In [6]–[10], a constellation-based M-ary DCSK system and its improved versions, where multiple binary information bits are converted into symbols, has been proposed to improve data rate and increase spectral efficiency. Recently, there have emerged many researches concentrating on combining DCSK with the most popular wireless communication technology, i.e., the multi-carrier modulation. As is well known, the multi-carrier modulation has many merits such as reliable in

The associate editor coordinating the review of this manuscript and approving it for publication was Lin Lin.

frequency-selecting fading channels, being compatible with other modulation technologies and easy to be implemented. Since a multi-carrier DCSK (MC-DCSK) system was proposed by G. Kaddoum in 2013 [11], various MC-DCSK systems have been designed [12]–[17]. Recently, as a promising high spectral-efficiency technology, index modulation is introduced to DCSK systems to further increase the data transmission rate and the spectral efficiency. Through index modulation, more information is embedded in the indices of the main components of the communication system, such as the subcarriers, orthogonal codes, transmit antennas, etc. Thus, the index modulation based DCSK system can provide higher spectral efficiency, higher data transmission rate and less energy consumption [18]–[22]. Especially, in [23], the media-based modulation technique (MBM), which is one of the newest index modulation technology, is introduced to the DCSK system to provide a significant increase in both spectral efficiency and data rate through implementing index modulation with reconfigurable antennas. Nowadays, there have been many researches combining M-ary modulation, multi carrier modulation and index modulation to further increase the data rate of the DCSK system [24]–[27].

For enhancing the security level of DCSK system, the research concentrates on eliminating the correlation between the reference and information-bearing signals. In [28]–[30], the authors proposed a reference-modulated DCSK scheme, in which the reference chaotic signal is also used to convey the information, to improve both the information security and the data rate. In [31] and [32], the similarity of the reference and information-bearing signal is reduced by a permutation matrix. The security of the OFDM-DCSK system is improved via frequency hopping, chaos masking or overlapped chaotic chip position shift keying in [5], [33], [34].

So far, increasing the data rate or spectral efficiency and enhancing the security level are still two popular topics for DCSK systems. The main drawback of MC-DCSK is that it requires large bandwidth [7]. What's more, the orthogonal DCSK systems have a strong dependence on the orthogonality of the carriers, which can be easily destroyed in a fast-varying channel. In addition, the complexity of the system is inevitably increased in most security-enhanced DCSK systems. Thus, in this paper, inspired by [35]–[38], we proposed a new high spectral efficiency DCSK system based on time-delay overlapping modulation, which is referred to as TDOP-DCSK, to achieve higher spectral efficiency, higher data rate and higher information security. In this design, the information is conveyed by multiple chaotic carriers, which are intentionally delayed in turn and directly overlapped in the time domain, and is demodulated through solving the corresponding equation system. The main contributions of this paper are as follows.

(1) A new high spectral efficiency DCSK system based on time-delay overlapping modulation is proposed. Through overlapping dozens of modulated chaotic carriers in no more than twice the symbol duration of DCSK, the spectral efficiency and data rate of are dramatically increased.

(2) The time-delay overlapping modulation reduces the correlation between the reference and information bearing chaotic signal, and therefore enhances the security level of DCSK.

(3) The spectral efficiency, energy efficiency, security, origin of error bit and the BER of TDOP-DCSK are analyzed. Then, the merits of TDOP-DCSK are verified by computer simulations.

The reminder of this paper is organized as follows. The system architecture of TDOP-DCSK and the principle of modulation and demodulation are demonstrated in Section II. In Section III, the system performance, such as the energy efficiency, spectral efficiency, security and complexity of the proposed system are analyzed. Then, the origin of error bits and the analytical BER expressions are derived in Section IV. The simulation results are given in Section V, and some conclusions are drawn in Section VI

II. SYSTEM MODEL

Fig 1 shows the system architecture of the proposed TDOP-DCSK. At the transmitter, the serial binary bit stream is firstly converted to N parallel data streams, and each data stream contains s bits. Then, each data stream is converted to the analog amplitude a_{i} (i$= 1 \ldots N$) according to the coding rule of Gray code. According to Fig. 2(a), a_{i} is selected from 2^{s} amplitudes which are uniformly distributed in the interval $[-V, +V]$, and each amplitude is set to be $\left(\frac{2m}{2^{\mathrm{s}}-1} - 1\right) V$, where $m = 0, 1, \ldots, 2^{\mathrm{s}} - 1$.

The chaotic sequence is generated by the logistic map, $x_{\mathrm{k}+1} = 1 - x_{\mathrm{k}}^2$. The length of the sequence is β, which is defined as the spreading factor. The generated chaotic sequence is divided into two paths. One serves as the reference signal $x_{\mathrm{r}}(t)$, and the other is used as the chaotic carrier to convey the information a_{i}. This chaotic carrier is again divided into N chaotic subcarriers and each chaotic subcarrier is initially delayed by τ related to its previous version, except for the first one. After modulating the information a_{i}, these chaotic subcarriers are directly added in time domain to finally form the information-bearing signal, which is expressed as

$$s(t) = \sum_{i=1}^{N} g_i(t - (i-1)\cdot\tau), \tag{1}$$

$$g_i(t - (i-1)\cdot\tau) = \begin{cases} a_i x(t - (i-1)\cdot\tau) & t \in T \\ 0 & t \notin T \end{cases}, \tag{2}$$

where T is the duration of the chaotic sequence and i$=1 \ldots N$. Different from [35], all the chaotic subcarriers of TDOP-DCSK are used to bear the information, and each subcarrier conveys a different amplitude a_{i}, thus a higher data rate is achieved. What's more, as all the chaotic subcarriers are generated from one chaotic sequence, the bandwidth of the whole TDOP-DCSK symbol is identical to that of a single chaotic subcarrier, which is referred to as B_{c}. Thus,

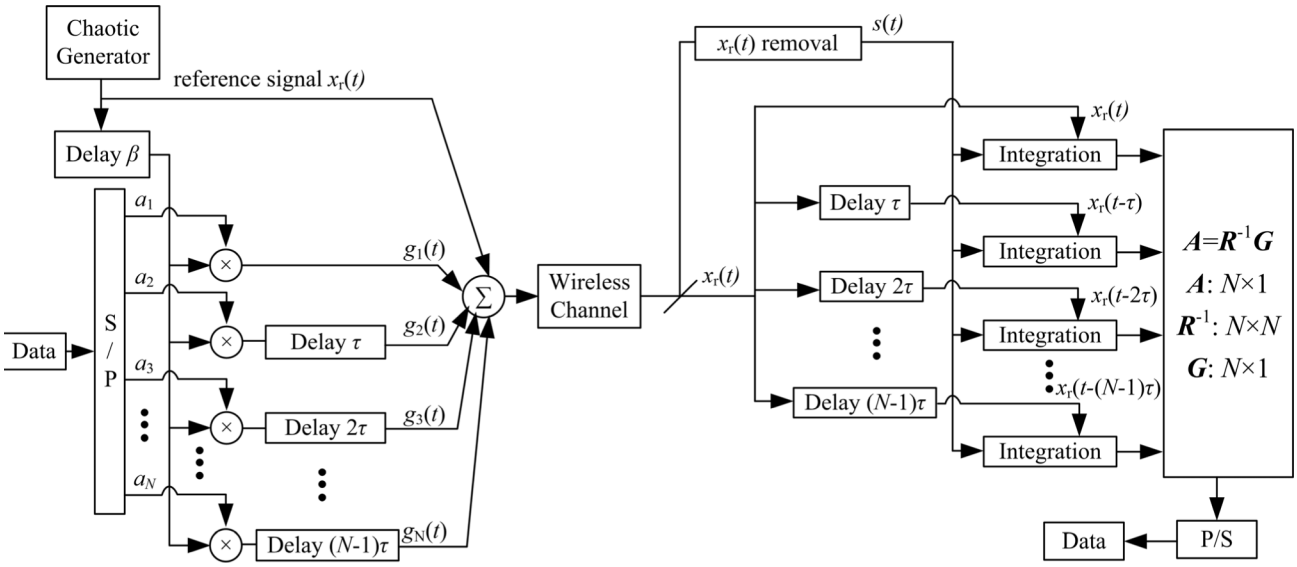

FIGURE 1. System model of TDOP-DCSK.

TDOP-DCSK can offer a higher spectral efficiency. Noting that, according to Fig. 2(b), the duration of the information bearing signal is extended due to multiple time-delays. In this paper, the duration of the information-bearing signal is default as 2β, and the whole symbol duration is 1.5 times of the traditional DCSK, as shown in Fig.2(b).

After modulation, the symbol is sent to the wireless channel. The model of the wireless channel is same to [17].

At the receiver, the reference and information-bearing signal are firstly separated. Then, a coherent computing is carried out between the reference and information-bearing signal, which is expressed as

$$\begin{aligned} G_1 &= \int_0^T s(t) \times x_r(t) dt \\ &= \int_0^T a_1 x(t) x_r(t)\, dt \\ &\quad + \int_0^T a_2 x(t-\tau) x_r(t)\, dt + \ldots \\ &\quad + \int_0^T a_N x(t-(N-1)\tau) x_r(t)\, dt \\ &= r_{11}a_1 + r_{12}a_2 + \ldots + r_{1N}a_N. \end{aligned} \tag{3}$$

Through (3) an equation for all the modulation amplitudes is obtained. Then, assuming the receiver already knows the time-delay information, the reference signal is delayed by τ and again used for a coherent computing with $s(t)$,

$$\begin{aligned} G_2 &= \int_0^T s(t) \times x_r(t-\tau) dt \\ &= \int_0^T a_1 x(t) x_r(t-\tau)\, dt \\ &\quad + \int_0^T a_2 x(t-\tau) x_r(t-\tau)\, dt + \ldots \\ &\quad + \int_0^T a_N x(t-(N-1)\tau) x_r(t-\tau)\, dt \\ &= r_{21}a_1 + r_{22}a_2 + \ldots + r_{2N}a_N. \end{aligned} \tag{4}$$

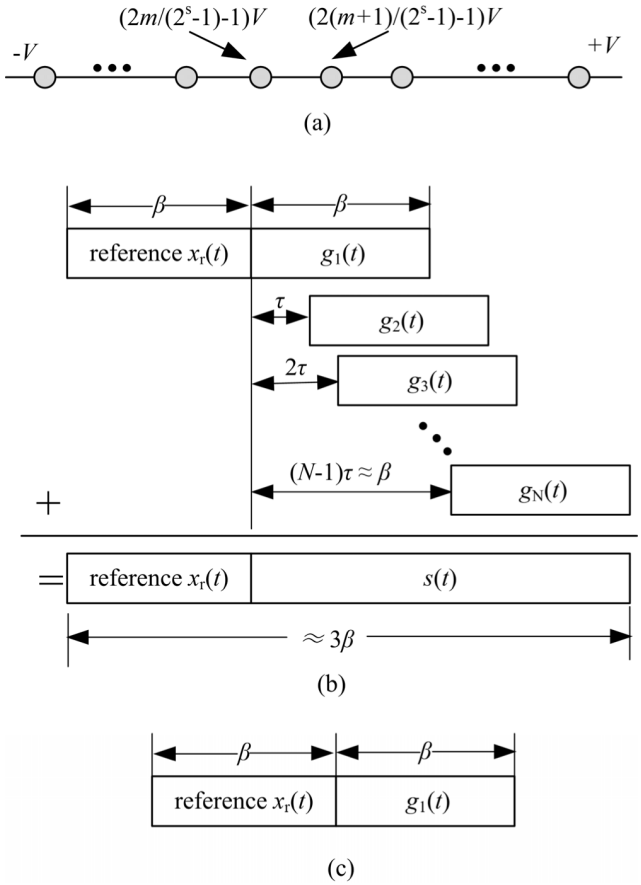

FIGURE 2. Symbol of TDOP-DCSK. (a) Distribution of analog amplitudes, (b) frame of TDOP-DCSK, (c) frame of the traditional DCSK.

After N times of time-delay and correlation computing, an equation system for modulation amplitudes can be obtained as

$$\boldsymbol{RA} = \boldsymbol{G}, \tag{5}$$

where

$$\boldsymbol{R} = \begin{bmatrix} r_{11} & r_{12} & \cdots & r_{1N} \\ r_{21} & r_{22} & \cdots & r_{2N} \\ \vdots & \vdots & \ddots & \vdots \\ r_{N1} & r_{N2} & \cdots & r_{NN} \end{bmatrix}$$

is a Toplize matrix, $\mathrm{A} = \begin{bmatrix} a_1 & a_2 & \ldots & a_N \end{bmatrix}^{\mathrm{T}}$ is the solution of the equation system whose elements are modulation amplitudes and $\mathrm{G} = \begin{bmatrix} G_1 & G_2 & \ldots & G_N \end{bmatrix}^{\mathrm{T}}$ Each modulation amplitude can be obtained through solving the equation system

$$\boldsymbol{A} = \boldsymbol{R}^{-1}\boldsymbol{G}. \tag{6}$$

Finally, the binary data stream is recovered via the coding rules at the transmitter.

As can be seen in (5) and (6), the demodulation process is to solve the equations set, and the bit error probability depends on the error of the solutions. Furthermore, the error of the solution is determined by the ill-condition of the equations set, and a high ill-condition will lead to a large error. This will be detailed in the following sections.

III. SYSTEM ANALYSIS

A. ENERGY EFFICIENCY AND SPECTRAL EFFICICENCY

The energy efficiency and spectral efficiency are both higher than those of the conventional DCSK. Firstly, in this paper, the data-energy-to-bit-energy ratio (DBR) is used to measure the energy efficiency. Similar to [11], the reference chaotic signal of TDOP-DCSK is shared by N modulated chaotic subcarriers, so

$$DBR_{\text{TDOP-DCSK}} = \frac{Energy_{data}}{Energy_b} = \frac{Energy_{data}}{Energy_{data} + \dfrac{Energy_{ref}}{N}} = \frac{N}{N+1}, \tag{7}$$

where $Energy_b$, $Energy_{data}$ and $Energy_{ref}$ are the energy of the transmitted bit, a single chaotic subcarrier and the reference signal, respectively. Obviously, $Energy_{data} = Energy_{ref}$.

When $N = 1$, (7) represents the energy efficiency of the traditional DCSK system, as shown in Fig. 2(c). According to (7), the DBR of traditional DCSK is

$$DBR_{DCSK} = \frac{Energy_{data}}{Energy_b} = \frac{Energy_{data}}{Energy_{data} + Energy_{ref}} = \frac{1}{2}. \tag{8}$$

To further investigate (7), the energy efficiency of TDOP-DCSK and MC-DCSK in [11] are shown in Fig. 3. According to [11], the DBR of the MC-DCSK system is

$$DBR_{MC-DCSK} = \frac{Energy_{data}}{Energy_b} = \frac{Energy_{data}}{Energy_{data} + \frac{Energy_{ref}}{N-1}}$$

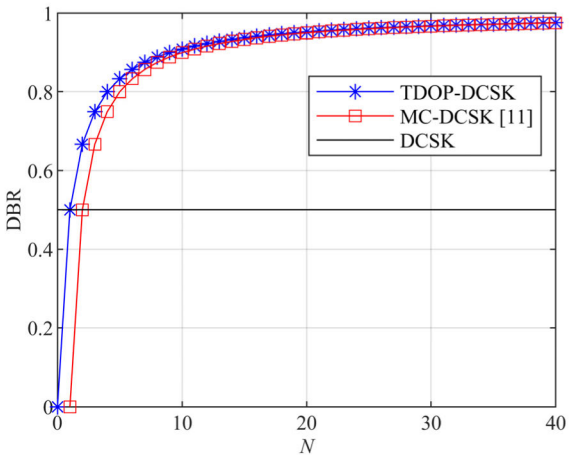

FIGURE 3. Energy efficiency of TDOP-DCSK, MC-DCSK and the traditional DCSK.

$$= \frac{N-1}{N}, \tag{9}$$

where N represents the number of subcarriers. When the number of chaotic subcarriers is low, the energy efficiency of TDOP-DCSK is higher than MC-DCSK. Additionally, when $N \geq 10$, the energy efficiency can reach up to more than 90%, which means that most of the bit energy is used to transmit the information bits, implying a higher energy efficiency.

As mentioned above, the bandwidth of the whole symbol of TDOP-DCSK is same with a single chaotic subcarrier B_c where $B_c = 1/T_c$ and T_c is the duration of a chip. Assuming each chaotic subcarrier conveys s bits, where $s \geq 1$, the symbol can transmit Ns bits. From Fig. 2(b), the duration of an TDOP-DCSK symbol is $3\beta T_c$, so the data rate is $R = Ns/(3\beta T_c)$. Therefore, the spectral efficiency (SE) of TDOP-DCSK is

$$SE_{TDOP-DCSK} = \frac{R_b}{B} = \frac{Ns/3\beta T_c}{1/T_c} = \frac{Ns}{3\beta}. \tag{10}$$

From (10), the SE of MC-TDOP-DCSK is proportional to the number of subcarriers N and the bits s that each subcarrier can convey, and is inversely proportional to the spreading factor β. To further demonstrate the superior of the proposed system, Fig. 4 shows the spectral efficiency of the proposed TDOP-DCSK, MC-DCSK and the traditional DCSK systems when β and s equal to 40 and 1, respectively According to [11], the SE of MC-DCSK is

$$SE_{MC-DCSK} = \frac{\frac{N-1}{\beta T_c}}{N\frac{1+\alpha}{T_c}} = \frac{N-1}{(1+\alpha)\,\beta N}, \tag{11}$$

where T_c is the chip time and is the rolloff factor satisfying the Nyquist criterion [11]. In addition, similar to the analysis of DBR, when both N and s equal to 1, (10) represents the SE of the traditional DCSK system and the $\mathrm{SE_{DCSK}}$ is $1/(3\beta)$. From Fig. 4, the SE of the proposed TDOP-DCSK system is higher than that of both MC-DCSK and the traditional DCSK. Thus, for the proposed TDOP-DCSK, N and s must be large

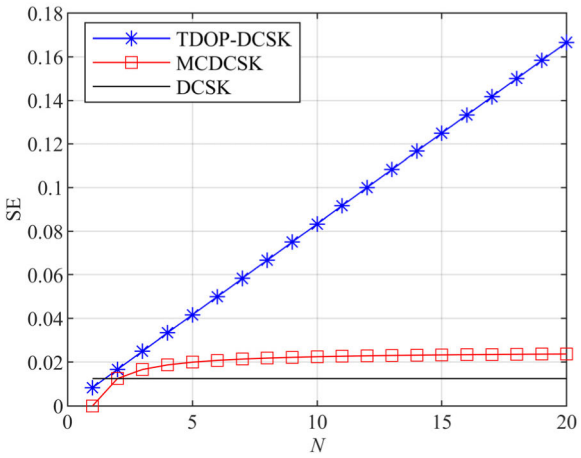

FIGURE 4. Spectral efficiency of TDOP-DCSK, MC-DCSK and the traditional DCSK.

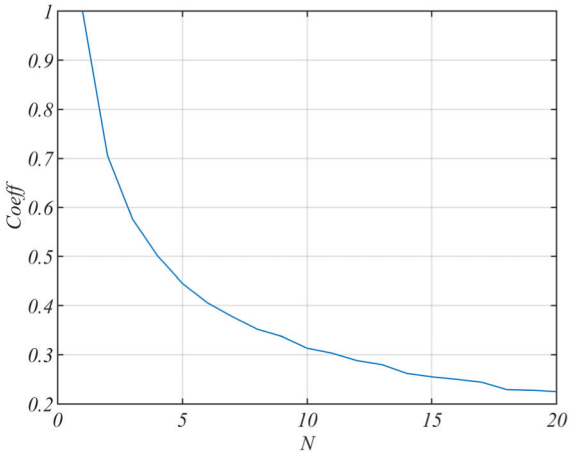

FIGURE 5. Correlation coefficient of the reference and information bearing signal.

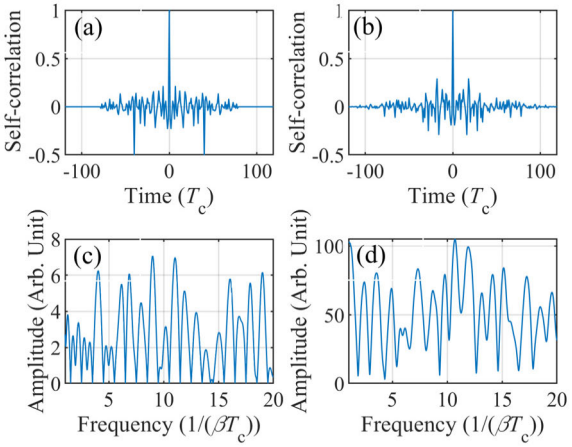

FIGURE 6. Self-correlation curve and energy spectrum of DCSK and MC-TDOP-DCSK. Left Column: DCSK, second column: MC-TDOP-DCSK.

to achieve a higher SE, and β must be small. Nevertheless, values of above parameters will influence the ill-condition of (6), so they must be appropriately optioned to ensure the BER performance.

B. SECURITY

In the traditional DCSK, the reference and information-bearing signal has a strong correlation, thus the security is weakened. In TDOP-DCSK, as the information-bearing signal is formed by many delayed chaotic subcarriers, the correlation can be significantly reduced. The correlation coefficient (CC) is selected to measure the correlation, which can be expressed as

$$Coeff = \int_{-\infty}^{\infty} x(\tau)\, s(t+\tau)\, d\tau. \tag{12}$$

Intuitively, according to Fig. 2(b), more chaotic subcarriers may reduce the correlation coefficient, so we explore the effect of N on the CC of the reference and information-bearing signal. The spreading factor β and chip duration T_c is set to be 40 and 25 ms, respectively. From Fig. 5, the CC is dramatically declined when N is large, which indicates a high level of security.

In addition, the spreading factor and the symbol rate information of DCSK can be easily extracted from the self-correlation curve and the energy spectrum. As clearly shown in Fig. 6(a) and (c), a correlation peak appears at $40T_c$, and the interval of the zero point is exactly the symbol rate of DCSK. However, for TDOP-DCSK, there is no correlation peak at the location of the spreading factor, and no zero point can be found from the energy spectrum, as shown in Fig. 6(b) and (d). Therefore, TDOP-DCSK has a higher security level.

C. COMPLEXITY

The complexity of the system is defined as the total number of multiplication and addition required for a system to transmit the data. For simplicity, transmit and receive antennas of all systems are set to be one. For the traditional DCSK system, β multiplications are required to transmit one bit at the transmitter. At the receiver, β multiplications and $\beta - 1$ additions are required to demodulate the received data. Therefore, the total complexity of the traditional DCSK system is $3\beta - 1$. For the index modulation based DCSK system, [23] for instance, 2β multiplications and β additions are required to transmit $(\log2(M_s) + \log2(N_l))$ bits, where M_s and N_l are the number of symbols and RF mirros. At the receiver, $M_s \times N_l$ multiplications are required for the ML detector to search the transmitted symbol and the indices. Thus the total complexity of the index modulation in [23] is $3\beta + M_s \times N_l$. In our system, $N\beta$ multiplications and $N-1$ additions are needed to transmit N bits. At the receiver, N multiplications are implemented to construct the equation set (5). Then, the transmitted data can be demodulated by solving (5). Therefore, the complexity of our system is $(\beta + 3)N - 1$. However, the complexity of the process of solving (5) is propotional to N^3. Finally, the complexity of our system is $O(N^3)$. Compared with the traditional DCSK system, the complexity is inevitably enhanced

in index modulation based DCSK and our TDOP-DCSK system, but much more bits are transmitted in the latter two systems.

IV. PERFORMANCE ANALYSIS

A. ORIGIN OF ERROR BITS

From (5), the error of the solution will directly influence the BER of TDOP-DCSK system. Let the error of the solution be $\Delta \boldsymbol{A}$, then (5) becomes

$$\boldsymbol{R}\left(\boldsymbol{A}+\Delta \boldsymbol{A}\right)=\boldsymbol{G}+\Delta \boldsymbol{G}, \tag{13}$$

where $\Delta \boldsymbol{G}$ is the error generated in the process of coherent computing. $\Delta \boldsymbol{G}$ is related to the noise and interference in the wireless channel. As (5) always hold, we have

$$\boldsymbol{R}\cdot \Delta \boldsymbol{A}=\Delta \boldsymbol{G}. \tag{14}$$

so

$$\Delta \boldsymbol{A}=\boldsymbol{R}^{-1}\Delta \boldsymbol{G}. \tag{15}$$

From (15), the BER is not only related to the noise and the multi-path interference, but also to $\boldsymbol{R}^{-1}$. According to the property of the norm, we have

$$\|\Delta \boldsymbol{A}\|\leq \left\|\boldsymbol{R}^{-1}\right\|\cdot \|\Delta \boldsymbol{G}\|. \tag{16}$$

From (16), $\Delta \boldsymbol{G}$ will be further affected by $\boldsymbol{R}^{-1}$. Therefore, $||\boldsymbol{R}^{-1}||$ must be as small as possible. From (1) to (4), the matrix $\boldsymbol{R}$ is formed by the chaotic subcarriers, which means the parameters of the symbol must be appropriately optioned.

B. DERIVATION OF BER EXPRESSIONS

1) AWGN CHANNEL

For the additive white Gaussian noise (AWGN) channel, the received signal is

$$\boldsymbol{r}=\boldsymbol{s}+\boldsymbol{n}, \tag{17}$$

where $\boldsymbol{n}$ denotes the noise. Then, (13) can be written as

$$\begin{aligned} R\left(\boldsymbol{A}+\Delta \boldsymbol{A}\right) &= \boldsymbol{G}+\Delta \boldsymbol{G} \\ &= \boldsymbol{C}^{\mathrm{H}}\left(\boldsymbol{s}+\boldsymbol{n}\right) \\ &= \boldsymbol{C}^{\mathrm{H}}\boldsymbol{s}+\boldsymbol{C}^{\mathrm{H}}\boldsymbol{n}, \end{aligned} \tag{18}$$

where

$$\boldsymbol{C}=\begin{pmatrix} x_r\left(t\right) \\ x_r\left(t-\tau\right) \\ \vdots \\ x_r\left(t-\left(N-1\right)\tau\right) \end{pmatrix}$$

From (5) and (18) we can get

$$\Delta \boldsymbol{G}=\boldsymbol{C}^{\mathrm{H}}\boldsymbol{n}. \tag{19}$$

so

$$\Delta \boldsymbol{A}=\boldsymbol{R}^{-1}\boldsymbol{C}^{\mathrm{H}}\boldsymbol{n}. \tag{20}$$

We can see that the error of the solution has the same distribution with that of the noise, that is

$$\mathrm{E}\left(\Delta \boldsymbol{A}\right)=0, \tag{21}$$

$$\begin{aligned} \mathrm{D}\left(\Delta \boldsymbol{A}\right) &= \boldsymbol{R}^{-1}\boldsymbol{C}^{\mathrm{H}}\boldsymbol{E}\left(\boldsymbol{n}\boldsymbol{n}^{\mathrm{H}}\right)C\left(\boldsymbol{R}^{-1}\right)^{\mathrm{H}} \\ &= \boldsymbol{P}_n\boldsymbol{R}^{-1}\boldsymbol{C}^{\mathrm{H}}\boldsymbol{C}\left(\boldsymbol{R}^{-1}\right)^{\mathrm{H}} \\ &= \boldsymbol{P}_n\boldsymbol{R}^{-1}, \end{aligned} \tag{22}$$

where P_{n} is the power of the noise E represents the expectation operator and D represents the variance operator. From (19), the elements in the diagonal of the matrix $\boldsymbol{R}^{-1}$ determine the anti-noise ability of TDOP-DCSK

From Fig. 2, the error bit appears when $\Delta \boldsymbol{A} > d$. Meanwhile, for the maximum and minimum amplitude, the bit error probability is half of the rest amplitudes. Thus, when all the amplitudes are sent with an equal probability, the average error rate of the ith modulation amplitude is

$$\begin{aligned} P_{ei} &= \frac{M-2}{NM}P\left(|\Delta \boldsymbol{A}|>d\right)+\frac{2}{NM}\cdot\frac{1}{2}P\left(|\Delta \boldsymbol{A}|>d\right) \\ &= \frac{M-1}{NM}P\left(|\Delta \boldsymbol{A}|>d\right). \end{aligned} \tag{23}$$

where $M = 2^s$ represents the total number of amplitudes as shown in Fig. 2(a). The error of the solution is a random variable whose mean value is 0 and variance is σ_{n}, so

$$P\left(|\Delta \boldsymbol{A}|>d\right)=\frac{2}{\sqrt{2\pi\psi_i}\sigma_n}\int_d^{\infty}e^{-x^2/2\psi_i\sigma_n^2}dx. \tag{24}$$

Substitute (24) into (23), we can get

$$\begin{aligned} P_{ei} &= \frac{M-1}{NM}\cdot\frac{2}{\sqrt{2\pi\psi_i}\sigma_n}\int_d^{\infty}e^{-x^2/2\psi_i\sigma_n^2}dx \\ &= \frac{M-1}{NM}erfc\left(\frac{d}{\sqrt{2\psi_i}\sigma_n}\right). \end{aligned} \tag{25}$$

Then, the relationship between the symbol power and the interval d must be found. As mentioned above, the values of analog amplitudes are $\left(\frac{2m}{2^s-1}-1\right)V$, so we can get $d = V/(M-1)$. The statistical properties of a_{i} are

$$E\left(a_{\mathrm{i}}\right)=0, \tag{26}$$

$$E\left(a_i^2\right)=\frac{V^2}{3}\left(\frac{M+1}{M-1}\right). \tag{27}$$

Then, the average power of the symbol is

$$\begin{aligned} P_s &= \frac{1}{T}\sum_{i=0}^{N-1}E\left(a_i^2\right)\int_0^T c_i^2\left(t\right)dt \\ &= \frac{NV^2}{3T}\left(\frac{M+1}{M-1}\right)P_c, \end{aligned} \tag{28}$$

where $P_c=\int_0^T c_i^2\left(t\right)dt$. Thus

$$d=\frac{V}{M-1}=\sqrt{\frac{3TP_s}{N\left(M^2-1\right)}\cdot\frac{1}{P_c}}. \tag{29}$$

Substituting (29) into (25), we can get the BER expression of TDOP-DCSK system,

$$P_e = \frac{M-1}{NM}\sum_{i=0}^{N-1} erfc\left(\sqrt{\frac{3T}{2N\psi_i\left(M^2-1\right)P_c}\cdot\frac{P_s}{P_n}}\right). \quad (30)$$

2) MULTI-PATH RAYLEIGH FADING CHANNEL

For multi-path Rayleigh fading channel, the received signal can be represented by

$$r(t) = \sum_{l=1}^{L}\lambda_l\left(t-\tau_l\right) * s(t) + n(t), \quad (31)$$

where L is the total number of paths, λ_l and τ_l are the channel coefficient and the time-delay of the l^{th} path, respectively.* is the convolution operator, and $n(t)$ is the AWGN

Then, the coherent computing between the reference and the information-bearing signal is (for mathematical simplification, the AWGN is neglected)

$$\begin{aligned} G_{1mp} &= \int_0^T r(t)\times x_r(t)\,dt \\ &= \int_0^T\left(\sum_{l=1}^{L}\lambda_l a_1 x\left(t-\tau_l\right)\right)x_r(t)\,dt \\ &\quad + \int_0^T\left(\sum_{l=1}^{L}\lambda_l a_2 x\left(t-\tau-\tau_l\right)\right)x_r(t)\,dt + \ldots \\ &\quad + \int_0^T\left(\sum_{l=1}^{L}\lambda_l a_N x\left(t-(N-1)\tau-\tau_l\right)\right)x_r(t)\,dt \\ &= r_{11mp}a_1 + r_{12mp}a_2 + \ldots + r_{1Nmp}a_N, \end{aligned} \quad (32)$$

where $r_{11mp} = \int_0^T\left(\sum_{l=1}^{L}\lambda_l x\left(t-\tau_l\right)\right)x_r(t)\,dt$, $r_{12mp} = \int_0^T\left(\sum_{l=1}^{L}\lambda_l x\left(t-\tau-\tau_l\right)\right)x_r(t)\,dt$, and so on, and the subscript mp represents the multi-path scenario. The remaining coherent computing processes are similar to (32). It can be seen that the multi-path interference is included in the elements of the matrix $\boldsymbol{R}$. Therefore, in (20), the elements of $\boldsymbol{R}^{-1}$ represent the multi-path interference. In this way, (30) is also suitable for multi-path Rayleigh fading channels.

V. NUMERICAL RESULTS

In this section, the performance of TDOP-DCSK over both AWGN and multi-path Rayleigh fading channels are numerically demonstrated. Effects of various system parameters on the BER performance are evaluated, and the comparison of BER performance between TDOP-DCSK and DCSK is also carried out to show the superior of TDOP-DCSK. The channel model is selected as a three-ray model with channel coefficients $E\left[\alpha_1^2\right] = 0.5$, $E\left[\alpha_2^2\right] = 0.4$, $E\left[\alpha_3^2\right] = 0.1$, and $\tau_1 = 0$, $\tau_2 = T_c$, $\tau_3 = 3T_c$ are the path delays.

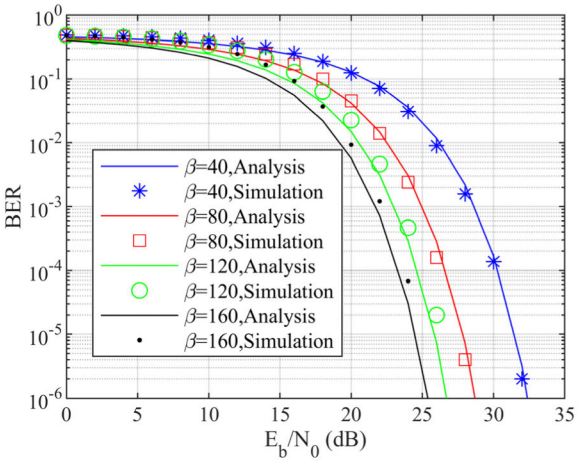

FIGURE 7. BER performance of TDOP-DCSK over AWGN channel with β = 40, 80, 120, 160, N = 16, and s = 1.

A. EFFECTS OF SYSTEM PARAMETERS ON BER PERFORMANCE

According to the theory of TDOP-DCSK, the parameters that can influence the performance are the spreading factor β, the number of chaotic subcarriers N and the bits s that each subcarrier conveys. Firstly, the influence of β on the BER performance over the AWGN channel and multi-path Rayleigh fading channel are shown in Fig. 7 and Fig. 8, respectively. β is set to be 40, 80, 120 and 160. We can see that a larger β will offer a better anti-noise ability, and the simulation results matches well with the analytical results. Furthermore, the norm of $\boldsymbol{R}^{-1}$ of each condition are calculated and shown in Tab 1. We can see that when β is large, the norm of $\boldsymbol{R}^{-1}$ is small, so the ill-condition is weakened and the BER is low, which matches well with previous theoretical inferences. From Fig. 7, 8 and Tab. 1, a larger β is necessary for a better BER performance.

According to Fig. 2(b), the symbol rate is proportional to the number of chaotic subcarriers N, so we investigate the effect of N on the BER performance. β is set to be 160, 240, 320, and N is 16, 32, 64, 128. From Fig. 9, for a fixed spreading factor, when N is large, the BER performance is deteriorated, which indicates a larger norm of $\boldsymbol{R}^{-1}$, as shown in Tab. 2. Notability, for a similar BER performance, when β is doubled, the number of subcarriers can also be doubled. For instance, as shown in the red circle in Fig. 8, $\beta = 160$, $N = 64$ and $\beta = 320$, $N = 128$ have similar BER performance, while the latter offers a higher data rate. Thus, to achieve a larger data rate, the spreading factor β must also be large.

Similarly, the parameter s, which refers to the bits that each subcarrier conveys, also determine the data rate of TDOP-DCSK. Fig. 10 shows BER performance of TDOP-DCSK for diverse s values. We can see that with the increasement of s the BER performance deteriorates. This is because when s is large, the interval of the amplitudes becomes small, indicating a weakened anti-noise and anti-interference ability. Meanwhile, for a fixed s value, the BER

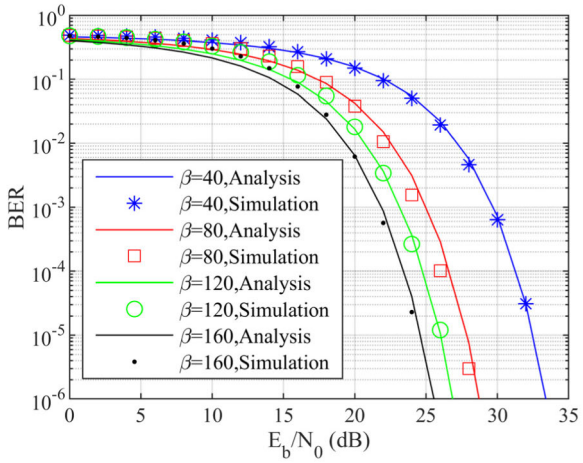

FIGURE 8. BER performance of TDOP-DCSK over multi-path Rayleigh fading channel with $\beta = 40, 80, 120, 160$, N = 16, and s = 1.

TABLE 1. Norm of $\boldsymbol{R}^{-1}$ for diverse spreading factor.

Channel Model	Spread factor	$\|\boldsymbol{R}^{-1}\|$
AWGN	40	0.1558
	80	0.0332
	120	0.0258
	160	0.0173
Multi-path	40	0.2070
	80	0.0367
	120	0.0243
	160	0.0180

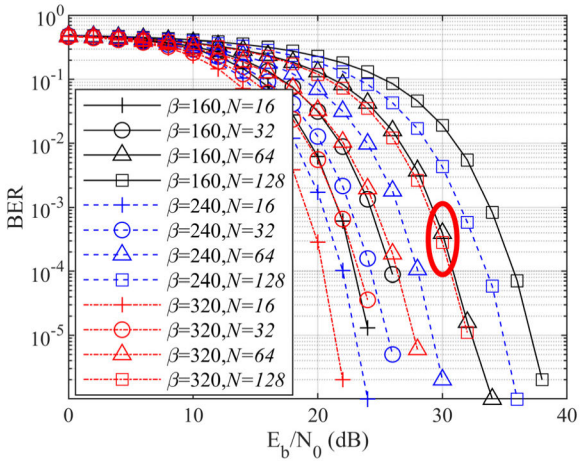

FIGURE 9. BER performance of TDOP-DCSK over multi-path Rayleigh fading channel with $\beta = 160, 240, 320$, N = 16, 32, 64, 128, and s = 1.

is lower for larger spreading factor β, which again implies that increasing β is an effective way to increase the data rate of TDOP-DCSK.

To further investigate the effect of N and s on the BER performance of TDOP-DCSK, we fix the symbol rate, which

TABLE 2. Norm of $\boldsymbol{R}^{-1}$ for diverse spreading factor and number of subcarriers.

Spreading factor	N	$\|\boldsymbol{R}^{-1}\|$
160	16	0.0179
	32	0.0274
	64	0.0673
	128	0.1923
240	16	0.0144
	32	0.0154
	64	0.0269
	128	0.1128
320	16	0.0111
	32	0.0174
	64	0.0231
	128	0.0581

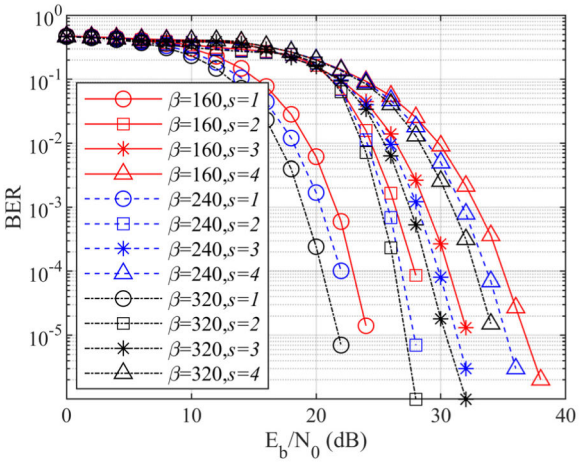

FIGURE 10. BER performance of TDOP-DCSK over multi-path Rayleigh fading channel with $\beta = 160, 240, 320$, N = 16, and s = 1, 2, 3, 4.

refers to total bits that a symbol conveys, and check the BER performance under diverse combinations of N and s. The spreading factor β is set to be 160. As clearly seen from Fig. 11, except for the case where symbol rate equals 32, the best BER performance appears when each chaotic subcarrier conveys 2 binary bits, i.e., s = 2. It is due to that when s is small, the N must consequently be large, and the ill-condition of (5) will accordingly be enhanced, leading to a worse BER performance. Besides, for a large s, the distribution of analog amplitudes will be denser and the interval between the amplitudes will consequently be narrower, implying a weakened anti-noise and anti-interference ability. Thus, for a specific symbol rate, one could set s to be 2 to achieve the best BER performance.

Finally, the results displayed above is under the hypothesis that the receiver already knows the time-delay parameter between each chaotic subcarrier. In fact, this parameter can be used as a key for TDOP-DCSK. Suppose there is an

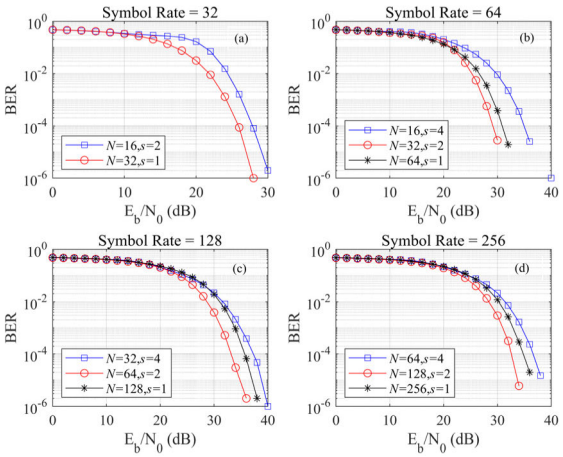

FIGURE 11. BER performance of TDOP-DCSK under diverse combinations of N and s, when the total symbol rate is fixed. (a) symbol rate = 32, (b) symbol rate = 64, (c) symbol rate = 128, (d) symbol rate = 256.

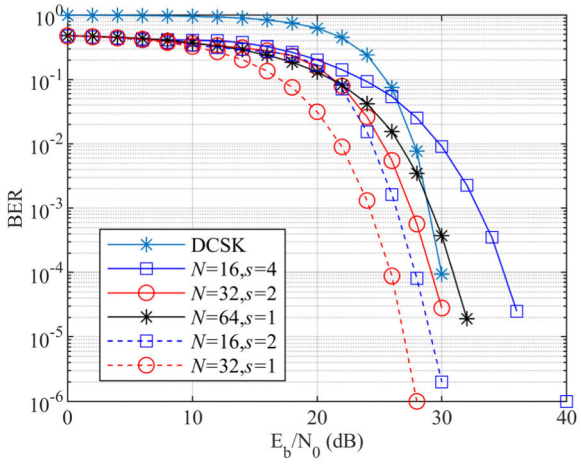

FIGURE 13. BER performance comparison between TDOP-DCSK under various parameter sets and traditional DCSK.

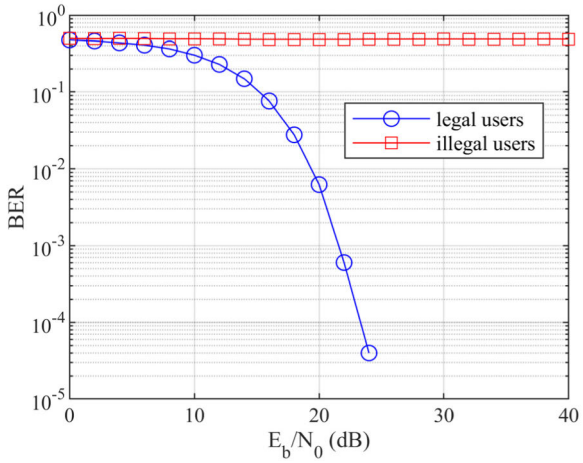

FIGURE 12. BER performance of TDOP-DCSK for legal and illegal users.

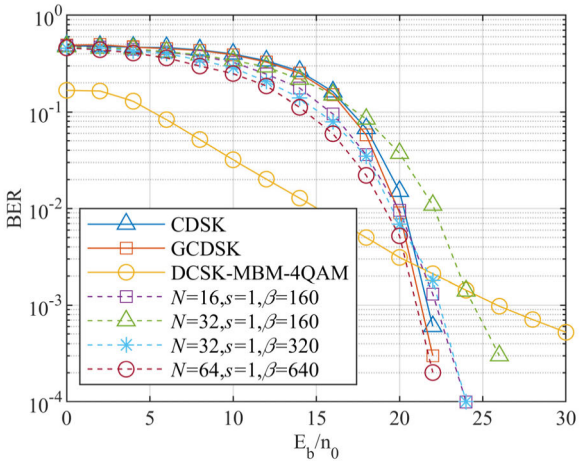

FIGURE 14. BER performance comparison between TDOP-DCSK under various parameter sets and other CSK versions, i. e. CDSK, GCDSK and MBM-DCSK.

eavesdropper who does not hold the time-delay parameter is trying to decode the message through (5). From Fig. 12, even the deviation of the time-delay parameter between legal and illegal user is $1T_c$, the BER of the illegal user is always nearly 50%, which means that the eavesdropper cannot correctly extract the information. Thus, together with Fig. 4 and Fig. 5, the security level is significantly enhanced by the time-delay overlapping modulation technology.

B. COMPARISON BETWEEN OTHER CHAOTIC COMMUNICATION SYSTEMS

Fig 13 shows the BER performance of traditional DCSK and the TDOP-DCSK under diverse parameter sets. The spreading factor β of both systems is set to be 160. When N equals to 32 and s equals to 1 and 2, the BER performance of TDOP-DCSK is always better than DCSK. Note that the symbol duration is 1.5 times of DCSK, when N and s equals to 32 and 2, respectively, the data rate of TDOP-DCSK is approximately 32*2/1.5≈40 times of DCSK. According to the BER analysis mentioned above, this data rate will further increase when β continues increase.

Finally, the BER performance of the proposed TDOP-DCSK system is compared with other chaos-shift-keying (CSK) systems, such as CDSK [38], GCDSK [35] and index modulation based DCSK [23] under different parameter sets. In CDSK and GCDSK, the information-bearing chaotic signal is also delayed and directly overlapped in time domain. The spreading factor β of CDSK, GCDSK and MBM-DCSK systems are all set to be 160. As shown in Fig. 14, for the same spreading factor, when N equals to 16, the BER performance of the TDOP-DCSK system is similar to CDSK and GCDSK. Noting that only one information bit is conveyed in a single CDSK or GCDSK symbol. That is to say, at this time, the symbol rate of TDOP-DCSK is 16 times of CDSK and GCDSK, which means a higher data transmission rate. When N equals to 32, the BER performance of TDOP-DCSK system is deteriorated. To achieve higher symbol rate, the spreading factor can be improved to decrease

the ill-condition of TDOP-DCSK. When β equals to 320 and 640, the symbol rate can reach up to 32 and 64 times of CDSK and GCDSK, while maintaining similar BER performances. Therefore, TDOP-DCSK offers merits such as higher spectral efficiency, higher data rate and higher level of security. It can also be observed from Fig. 14 that the MBM-DCSK has a stronger anti-noise ability at low E_b/N regime, meanwhile provides high spectral efficiency and data rate. This implies that the index modulation technology will provide a better performance when the power of the signal is low and we get a hypothesis that combining index modulation technology with our proposed system will further improve the performance. It is interesting and will be our future work.

VI. CONCLUSION

In this paper, a new high spectral efficiency DCSK system based on time-delay overlapping modulation is proposed. The modulation and demodulation theory are demonstrated, and the system performance is analyzed through both theoretical deviation and computer simulation. The results show that the TDOP-DCSK system can offer a higher data rate, a higher spectral efficiency, and a higher security level. The spreading factor β is the crucial parameter in TDOP-DCSK, because a larger β brings better BER performance and a higher data rate. Meanwhile, the bandwidth of an TDOP-DCSK symbol is equal to that of a single chaotic subcarrier, indicating a higher spectral efficiency. In addition, benefiting from the time-delay overlapping method, the security of the whole system is significantly enhanced. Finally, compared to the tradition DCSK system, the data rate of TDOP-DCSK can be increased more than 40 times.

It is worth noting that the proposed TDOP-DCSK applies a ''time delay'' idea to construct the symbol. As a result, it will inevitably introduce latency to the whole communication system, because the duration of a symbol is increased. However, this latency can be optimized by several means, such as enhancing the sampling rate and reducing the ''time delay'' parameter τ shown in Fig. 2(b). Thus, future work will concentrate on controlling the system parameters to further improve the spectral efficiency, data rate and security level of TDOP-DCSK, and discovering methods to optimize the latency of the whole system.

REFERENCES

[1] G. Kaddoum, ''Wireless chaos-based communication systems: A comprehensive survey,'' *IEEE Access*, vol. 4, pp. 2621–2648, May 2016.
[2] Y. Fang, G. Han, P. Chen, F. C. M. Lau, G. Chen, and L. Wang, ''A survey on DCSK-based communication systems and their application to UWB scenarios,'' *IEEE Commun. Surveys Tuts.*, vol. 18, no. 3, pp. 1804–1837, 3rd Quart., 2016.
[3] G. Kaddoum and N. Tadayon, ''Differential chaos shift keying: A robust modulation scheme for power-line communications,'' *IEEE Trans. Circuits Syst. II, Exp. Briefs*, vol. 64, no. 1, pp. 31–35, Jan. 2017.
[4] N. X. Quyen, ''Quadrature MC-DCSK scheme for chaos-based cognitive radio,'' *Int. J. Bifurcation Chaos*, vol. 29, no. 13, pp. 1950177-1–1950177-15, 2019.
[5] L. Zhang, Z. Chen, W. Rao, and Z. Wu, ''Efficient and secure non-coherent OFDM-based overlapped chaotic chip position shift keying system: Design and performance analysis,'' *IEEE Trans. Circuits Syst. I, Reg. Papers*, vol. 67, no. 1, pp. 309–321, Jan. 2020.
[6] L. Wang, G. Cai, and G. R. Chen, ''Design and performance analysis of a new multiresolution M-ary differential chaos shift keying communication system,'' *IEEE Trans. Wireless Commun.*, vol. 14, no. 9, pp. 5197–5208, Sep. 2015.
[7] G. Cai, Y. Fang, G. Han, C. M. F. Lau, and L. Wang, ''A square-constellation-based M-ary DCSK communication system,'' *IEEE Access*, vol. 4, pp. 6295–6303, Oct. 2016.
[8] G. Cai and Y. Song, ''Closed-form BER expressions of M-ary DCSK systems over multipath Rayleigh fading channels,'' *IEEE Commun. Lett.*, vol. 24, no. 6, pp. 1192–1196, Jun. 2020.
[9] M. Miao, L. Wang, G. Chen, and W. Xu, ''Design and analysis of replica piecewise M-ary DCSK scheme for power line communications with asynchronous impulsive noise,'' *IEEE Trans. Circuits Syst. I, Reg. Papers*, vol. 67, no. 12, pp. 5443–5453, Dec. 2020.
[10] H. Ma, G. Cai, Y. Fang, P. Chen, and G. Chen, ''Design of a superposition coding PPM-DCSK system for downlink multi-user transmission,'' *IEEE Trans. Veh. Technol.*, vol. 69, no. 2, pp. 1666–1678, Feb. 2020.
[11] G. Kaddoum, F. Richardson, and F. Gagnon, ''Design and analysis of a multi-carrier differential chaos shift keying communication system,'' *IEEE Trans. Commun.*, vol. 61, no. 8, pp. 3281–3291, Aug. 2013.
[12] H. Yang, W. K. S. Tang, G. Chen, and G.-P. Jiang, ''Multi-carrier chaos shift keying: System design and performance analysis,'' *IEEE Trans. Circuits Syst. I, Reg. Papers*, vol. 64, no. 8, pp. 2182–2194, Aug. 2017.
[13] G. Kaddoum, ''Design and performance analysis of a multiuser OFDM based differential chaos shift keying communication system,'' *IEEE Trans. Commun.*, vol. 64, no. 1, pp. 249–260, Jan. 2016.
[14] Z. Liu, L. Zhang, and Z. Chen, ''Low PAPR OFDM-based DCSK design with carrier interferometry spreading codes,'' *IEEE Commun. Lett.*, vol. 22, no. 8, pp. 1588–1591, Aug. 2018.
[15] H. Zhou, Y. Zhang, and Y. Yu, ''Noise reduction multi-carrier differential chaos shift keying system,'' *J. Circuit Syst. Comput.*, vol. 27, no. 14, pp. 1850233-1–1850233-16, May 2018.
[16] N. X. Quyen, ''Multi-carrier differential chaos-shift keying with repeated spreading sequence,'' *J. Commun. Netw.*, vol. 20, no. 3, pp. 299–308, Jun. 2018.
[17] B. Chen, L. Zhang, and Z. Wu, ''General iterative receiver design for enhanced reliability in multi-carrier differential chaos shift keying systems,'' *IEEE Trans. Commun.*, vol. 67, no. 11, pp. 7824–7839, Nov. 2019.
[18] G. Cheng, L. Wang, W. Xu, and G. Chen, ''Carrier index differential chaos shift keying modulation,'' *IEEE Trans. Circuits Syst. II, Exp. Briefs*, vol. 64, no. 8, pp. 907–911, Aug. 2017.
[19] W. Xu, Y. Tan, F. C. M. Lau, and G. Kolumbán, ''Design and optimization of differential chaos shift keying scheme with code index modulation,'' *IEEE Trans. Commun.*, vol. 66, no. 5, pp. 1970–1980, May 2018.
[20] W. Xu, T. Huang, and L. Wang, ''Code-shifted differential chaos shift keying with code index modulation for high data rate transmission,'' *IEEE Trans. Commun.*, vol. 65, no. 10, pp. 4285–4294, Oct. 2017.
[21] Y. Tan, W. Xu, T. Huang, and L. Wang, ''A multilevel code shifted differential chaos shift keying scheme with code index modulation,'' *IEEE Trans. Circuits Syst. II, Exp. Briefs*, vol. 65, no. 11, pp. 1743–1747, Nov. 2018.
[22] F. Cogen, E. Aydin, N. Kabaoglu, E. Basar, and H. Ilhan, ''Generalized code index modulation and spatial modulation for high rate and energy-efficient MIMO systems on Rayleigh block-fading channel,'' *IEEE Syst. J.*, vol. 15, no. 1, pp. 538–545, Mar. 2021.
[23] B. Onal, F. Cogen, and E. Aydin, ''Differential chaos shift keying-assisted media-based modulation,'' *Electrica*, vol. 21, no. 1, pp. 66–73, Jan. 2021.
[24] G. Cai, Y. Fang, J. Wen, S. Mumtaz, Y. Song, and V. Frascolla, ''Multi-carrier M-ary DCSK system with code index modulation: An efficient solution for chaotic communications,'' *IEEE J. Sel. Topics Signal Process.*, vol. 13, no. 6, pp. 1375–1386, Oct. 2019.
[25] G. Cai, Y. Fang, P. Chen, G. Han, G. Cai, and Y. Song, ''Design of an MISO-SWIPT-aided code-index modulated multi-carrier M-DCSK system for E-health IoT,'' *IEEE J. Sel. Areas Commun.*, vol. 39, no. 2, pp. 311–324, Feb. 2021.
[26] T. Huang, L. Wang, W. Xu, and G. Chen, ''A multi-carrier M-ary differential chaos shift keying system with low PAPR,'' *IEEE Access*, vol. 5, pp. 18793–18803, Oct. 2017.
[27] X. Cai, W. Xu, L. Wang, and G. Kolumbán, ''Multicarrier M-ary orthogonal chaotic vector shift keying with index modulation for high data rate transmission,'' *IEEE Trans. Commun.*, vol. 68, no. 2, pp. 974–986, Feb. 2020.
[28] H. Yang and G.-P. Jiang, ''High-efficiency differential-chaos-shift-keying scheme for chaos-based noncoherent communication,'' *IEEE Trans. Circuits Syst. II, Exp. Briefs*, vol. 59, no. 5, pp. 312–316, May 2012.

[29] H. Yang and G.-P. Jiang, "Reference-modulated DCSK: A novel chaotic communication scheme," *IEEE Trans. Circuits Syst. II, Exp. Briefs*, vol. 60, no. 4, pp. 232–236, Apr. 2013.
[30] H. Yang, G. Jiang, L. Xia, and X. Tu, "Reference-shifted DCSK modulation scheme for secure communication," in *Proc. Int. Conf. Comput., Netw. Commun. (ICNC)*, Silicon Valley, CA, USA, Jan. 2017, pp. 1073–1076.
[31] F. C. M. Lau, K. Y. Cheong, and C. K. Tse, "Permutation-based DCSK and multiple-access DCSK systems," *IEEE Trans. Circuits Syst. I, Fundam. Theory Appl.*, vol. 50, no. 6, pp. 733–742, Jun. 2003.
[32] M. Herceg, G. Kaddoum, D. Vranješ, and E. Soujeri, "Permutation index DCSK modulation technique for secure multiuser high-data-rate communication systems," *IEEE Trans. Veh. Technol.*, vol. 67, no. 4, pp. 2997–3011, Apr. 2018.
[33] Z. Liu, L. Zhang, Z. Wu, and J. Bian, "A secure and robust frequency and time diversity aided OFDM-DCSK modulation system not requiring channel state information," *IEEE Trans. Commun.*, vol. 68, no. 3, pp. 1684–1697, Mar. 2020.
[34] Z. Liu, L. Zhang, and Z. Wu, "Reliable and secure pre-coding OFDM-DCSK design for practical cognitive radio systems with the carrier frequency offset," *IEEE Trans. Cognit. Commun. Netw.*, vol. 6, no. 1, pp. 189–200, Mar. 2020.
[35] W. M. Tam, F. C. M. Lau, and C. K. Tse, "Generalized correlation-delay-shift-keying scheme for noncoherent chaos-based communication systems," *IEEE Trans. Circuits Syst. I, Reg. Papers*, vol. 53, no. 3, pp. 712–721, Mar. 2006.
[36] M. He, D. Liang, and Q. Cao, "A modulation with higher bandwidth efficiency than OFDM," in *Proc. ICSPS*, Dalian, China, 2010, pp. VI-393–VI-397.
[37] Q. Cao and D. Liang, "Study on modulation techniques free of orthogonality restriction," *Sci. China F, Inf. Sci.*, vol. 50, no. 6, pp. 889–896, Dec. 2007.
[38] M. Sushchik, L. S. Tsimring, and A. R. Volkovskii, "Performance analysis of correlation-based communication schemes utilizing chaos," *IEEE Trans. Circuits Syst. I, Fundam. Theory Appl.*, vol. 47, no. 12, pp. 1684–1691, Dec. 2000.

XINYU DOU was born in Shenyang, Liaoning, China, in 1987. He received the B.S. degree in optical information science and technology and the Ph.D. degree in communication engineering from Dalian University of Technology, Dalian, in 2010 and 2016, respectively.

From 2019 to 2021, he was a Postdoctoral Fellow with the Information and Communication Engineering, Dalian Maritime University, China. He is currently a Full Lecturer with the College of Information Science and Technology, Dalian Maritime University. His research interests include wireless communications chaos-based wireless and optical communications and neuromorphic photonics.

XIAOHUI CHEN received the B.S. degree in communication engineering from Weifang University, Weifang, China, in 2018. He is currently pursuing the M.S. degree with the College of Information Science and Technology, Dalian Maritime University, Dalian, China. His research interests include chaos-based digital communications and their applications to wireless communications.

DEQUN LIANG received the B.S. degree from Xi'an Jiaotong University, Xi'an, China, in 1966. From 1966 to 1998, he was a Full Lecturer, a Full Associate Professor, and a Full Professor with Xi'an Jiaotong University. From 1988 to 1989, he was a Senior Visiting Scholar with the University of Manchester Institute of Science and Technology. From 1998 to 2011, he was a Full Professor with the College of Information Science and Technology, Dalian Maritime University. He is the author of one book, more than 150 articles, and 14 patents. His research interests include wireless communications, pattern recognition, image processing, and artificial intelligence.

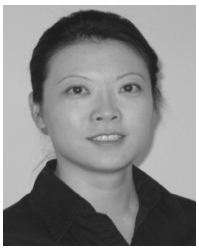

BIN LIN (Senior Member, IEEE) received the B.S. and M.S. degrees from Dalian Maritime University, Dalian, China, in 1999 and 2003, respectively, and the Ph.D. degree from the Broadband Communications Research Group, Department of Electrical and Computer Engineering, University of Waterloo, Waterloo, ON, Canada, in 2009. She has been a Visiting Scholar with George Washington University, Washington, DC, USA, from 2015 to 2016. She is currently a Full Professor and the Dean of the Department of Communication Engineering, College of Information Science and Technology, Dalian Maritime University. Her current research interests include wireless communications, network dimensioning and optimization, resource allocation, artificial intelligence, maritime communication networks, edge/cloud computing, wireless sensor networks, and the Internet of Things. She is an Associate Editor of IEEE TRANSACTION ON VEHICULAR TECHNOLOGY and *IET Communications*.